

# Geophysical Research Letters®

## RESEARCH LETTER

10.1029/2021GL097573

### Key Points:

- Fine structures of an electron current sheet in the electron diffusion region are presented
- The formation of these structures are closely related to the streaming and meandering electrons
- The low frequency fluctuation of this current sheet is also revealed

### Supporting Information:

Supporting Information may be found in the online version of this article.

### Correspondence to:

B.-B. Tang and W. Y. Li,  
[bbtang@spaceweather.ac.cn](mailto:bbtang@spaceweather.ac.cn);  
[wyli@spaceweather.ac.cn](mailto:wyli@spaceweather.ac.cn)









### Citation:

Tang, B.-B., Li, W. Y., Khotyaintsev, Y. V., Graham, D. B., Gao, C. H., Chen, Z. Z., et al. (2022). Fine structures of the electron current sheet in magnetotail guide-field reconnection. *Geophysical Research Letters*, 49, e2021GL097573. <https://doi.org/10.1029/2021GL097573>

Received 22 DEC 2021

Accepted 23 APR 2022

## Fine Structures of the Electron Current Sheet in Magnetotail Guide-Field Reconnection

B.-B. Tang<sup>1</sup> , W. Y. Li<sup>1</sup> , Yu. V. Khotyaintsev<sup>2</sup> , D. B. Graham<sup>2</sup> , C. H. Gao<sup>1,3</sup>, Z. Z. Chen<sup>4</sup> , H. S. Fu<sup>4</sup> , Q. M. Lu<sup>5</sup> , C. Wang<sup>1,3</sup>, and J. L. Burch<sup>6</sup> 

<sup>1</sup>State Key Laboratory of Space Weather, National Space Science Center, Chinese Academy of Sciences, Beijing, China,

<sup>2</sup>Swedish Institute of Space Physics, Uppsala, Sweden, <sup>3</sup>College of Earth and Planetary Sciences, University of Chinese Academy of Sciences, Beijing, China, <sup>4</sup>School of Space and Environment, Beihang University, Beijing, China, <sup>5</sup>CAS

Key Laboratory of Geospace Environment, Department of Geophysics and Planetary Science, University of Science and Technology of China, Hefei, China, <sup>6</sup>Southwest Research Institute, San Antonio, TX, USA

**Abstract** We investigate fine structures of the electron current sheet in magnetotail guide-field reconnection using Magnetospheric Multiscale observations. This current sheet, observed in the outer electron diffusion region (EDR) of reconnection, is featured by clear bifurcation and deflection, and also has complicated fine sublayers. The formation of these sublayers is closely related to streaming and meandering electrons, which are facilitated by the reconnection guide field. In particular, in the sublayer around the  $B_L$  reversal, the meandering electrons, which usually move along the out-of-plane (M) direction, are strongly distorted into the  $v_L$ - $v_N$  plane due to the finite  $B_M$  component. The low frequency fluctuation of this current sheet is also revealed, contributing  $\sim 3\%$  of the reconnection electric field by the anomalous effect. We suggest that such current sheet fluctuations, possibly driven by the magnetic double-gradient instability, can be characteristic in the outer EDR.

**Plain Language Summary** The electron-scale current sheet forms a basic feature of the electron diffusion region of magnetic reconnection, in which the topology of magnetic field lines changes and various electron processes occur. However, owing to its thinness, the fine structure of the electron current sheet has not been fully investigated, despite some general configurations having been reported. In this study, by using high-resolution measurements from Magnetospheric Multiscale mission, we present fine structures of an electron current sheet in guide-field reconnection, and show how these fine structures are closely related to the electron motion. Besides, the low frequency fluctuation of this current sheet is also revealed. These results provide new insight to reconnection dynamics at electron scales.

## 1. Introduction

Magnetic reconnection is a fundamental process that changes magnetic field topologies, and converts magnetic energy into plasma energy. Though the consequences of reconnection can be large scale, electron-scale physics play an important role in the reconnection X-line region, where electrons are decoupled from the magnetic field lines, and the divergence of the electron off-diagonal pressure tensor is suggested to balance the reconnection electric field in the absence of turbulence (i.e., Cai & Lee, 1997; Egedal et al., 2019; Kuznetsova et al., 2001). The region where the electron frozen-in condition is violated is named as the electron diffusion region (EDR). Intense currents primarily carried by electrons are often found in the EDR (Burch et al., 2016; Khotyaintsev et al., 2016; Li et al., 2020; Torbert et al., 2018; Wang, Wang, et al., 2021; Zhou et al., 2019, and reference therein), and such thin electron current sheet has also been taken as a typical feature of EDRs (Fuselier et al., 2017; Webster et al., 2018).

The configuration of the electron current sheet is associated with electron dynamics. It can extend tens of ion inertial lengths downstream from the X-line with the electron jet (Phan et al., 2007). This elongation is affected by the reconnection guide field  $B_g$  and the electron  $\beta$  (ratio of the electron thermal pressure to the magnetic pressure) as shown by kinetic simulations (Le et al., 2013). Meanwhile, due to the electron meandering/bouncing motion around the  $B_L$  reversal, the electron out-of-plane velocity presents a double-peak structure, leading into the electron current sheet bifurcation (Chen et al., 2011; Huang et al., 2020; Swisdak et al., 2005). When a finite guide field is present, the electron current sheet is deflected by the  $J_L \times B_g$  force, and the deflection can be evident

even if  $B_g$  is weak (Goldman et al., 2011; Zhou et al., 2014). These results show the complexity of the electron current sheet structure, which varies significantly under different reconnection parameters. This can be explained by that the electron dynamics such as magnetization/demagnetization are sensitive to these parameters (e.g., Chen et al., 2019; Le et al., 2013; Swisdak et al., 2005), and the related electron motion forms different current sheets. Recently, with high resolution measurements from Magnetospheric Multiscale (MMS) mission (Burch et al., 2016), inhomogeneous structures of an EDR has been presented (Cozzani et al., 2019), but what the fine structures of an electron current sheet could be remains an open question.

In this study, we present fine structures of an electron current sheet in magnetotail reconnection with a guide field of  $\sim 0.1$  by using MMS data. We show how the beam and meandering electrons form complicated sublayers even inside an electron-scale current sheet. Finally, the fluctuation of this current sheet is also revealed, contributing  $\sim 3\%$  of the reconnection electric field by the anomalous effect.

## 2. Observation

We present MMS observations at Earth's magnetotail on 27 August 2018, and we use magnetic field data from the fluxgate magnetometer (Russell et al., 2016), electric field data from the electric field double probes (Ergun et al., 2016; Lindqvist et al., 2016), and particle data from the fast plasma investigation (Pollock et al., 2016). Due to the flight anomaly of electron spectrometer at MMS 4, electron data of MMS 4 are not shown here. On 27 August 2018, MMS spacecraft stay near the magnetotail current sheet for a long time. An X-line encounter with large amplitude upper hybrid waves is recorded around 11:41:26 UT (Li et al., 2021), and about 35 min later, MMS cross the magnetotail current sheet again, which is the focus of this study.

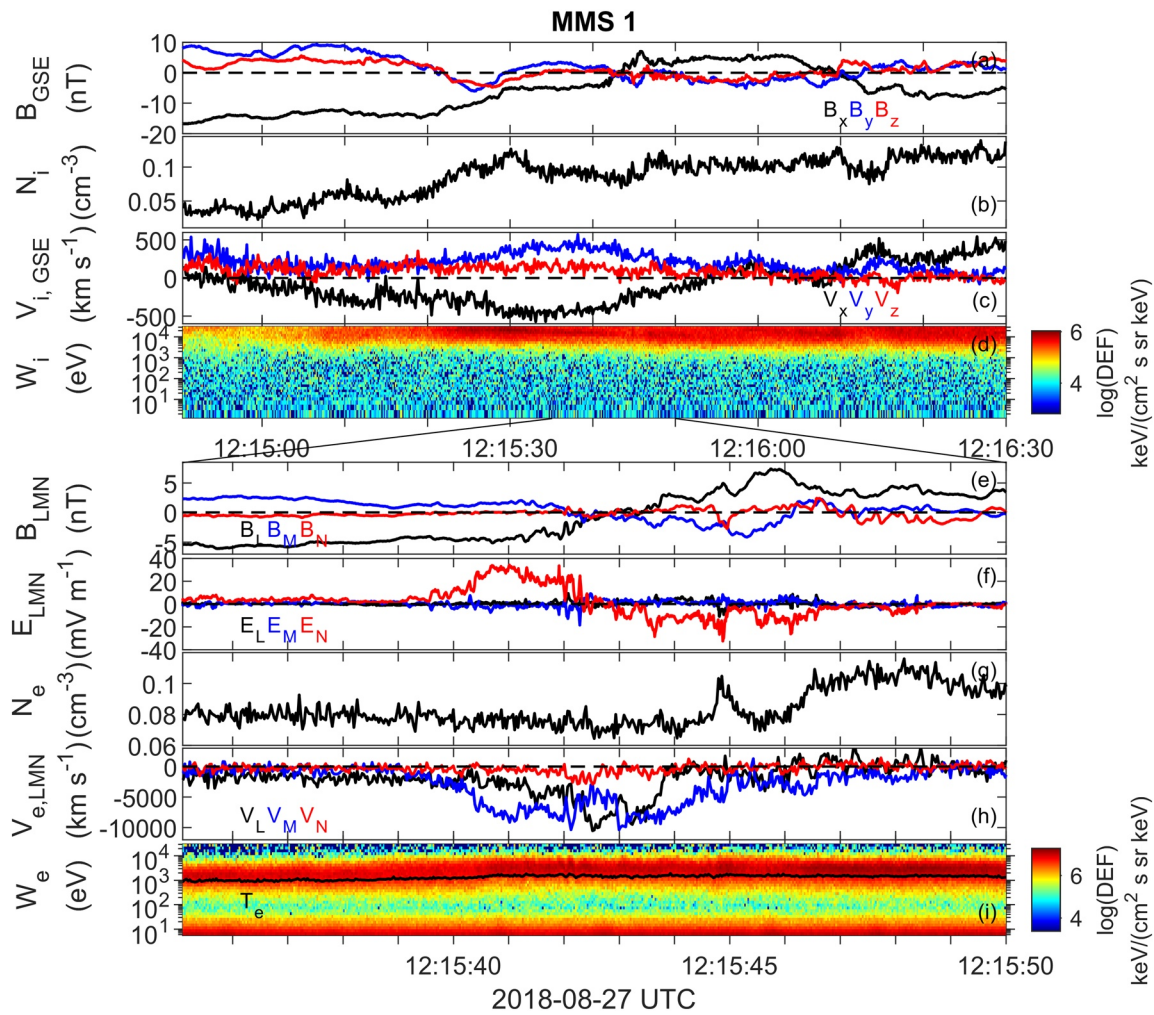
### 2.1. Overview

Figure 1 provides an overview of the magnetotail current sheet crossing between 12:14:50 UT and 12:16:30 UT. At this time, the four MMS spacecraft is located at  $[-21.07, 10.82, 9.07]$  Earth radii ( $R_E$ ) in geocentric solar ecliptic (GSE) coordinates, and the spacecraft are in a tetrahedron formation with  $\sim 34$  km separation. The negative-positive change of  $B_x$  at 15:15:43 UT indicates MMS move from the southern side of the magnetotail current sheet to the northern side, and MMS return to the southern side around 15:16:09 UT (Figure 1a). Around the first  $B_x$  reversal, MMS also observe the ion flow reversal of  $V_x$  (Figure 1c), suggesting ongoing magnetic reconnection. The negative-positive change of  $V_x$  indicates the tailward retreating of the reconnection X-line.

A zoom-in of the magnetotail current sheet crossing is presented in boundary-normal (LMN) coordinates, which is determined by a hybrid variance analysis method. The normal direction ( $\mathbf{N}'$ ) is along the minimum variance direction of the current density (12:15:38 UT to 12:15:46 UT), and the  $\mathbf{M}$  direction is from  $\mathbf{N}' \times \mathbf{L}$ , where  $\mathbf{L}$  is the direction of maximum variance of the magnetic field (12:15:15 UT to 12:15:50 UT). Finally,  $\mathbf{N} = \mathbf{L} \times \mathbf{M}$ . In GSE, it gives  $\mathbf{L} = [0.99, -0.12, -0.11]$ , and  $\mathbf{M} = [0.15, 0.96, 0.25]$  and  $\mathbf{N} = [0.08, -0.26, 0.96]$ , respectively. The magnetic  $B_M$  component changes from positive to negative (Figure 1e), consistent with the Hall pattern of reconnection, and MMS cross the reconnection region from its tailside. The magnitude of  $B_M$  at the  $B_L$  reversal is about  $-1.5$  nT, indicating a guide field  $\sim 0.1$  times of the asymptotic reconnecting field ( $\sim 15$  nT, Figure 1a). Meanwhile, MMS observe strong bipolar Hall electric fields (Figure 1f), and fast electron bulk flows in both  $-L$  and  $+M$  directions, reaching  $10,000$  km  $s^{-1}$  (Figure 1h). The electron bulk flow outruns the  $\mathbf{E} \times \mathbf{B}$  convection speed (not shown), suggesting demagnetization of electrons. In fact, an EDR is identified here, and an electron-scale flux rope embedded in this EDR is found at 12:15:44.75 UT (Z. Chen et al., 2021).

### 2.2. Fine Structure of the Electron Current Sheet

More details of this EDR crossing are provided by joint observations of four MMS spacecraft, in which MMS 4 is the leading one as shown by  $B_L$  (Figure 2b). In the shaded magenta region, the magnetic  $B_N$  component is enhanced, and the largest  $B_N$  is recorded by MMS 4, reaching to  $\sim -1.7$  nT (Figure 2d). Noticing that the positive  $E_N$  at MMS is much weaker than that observed by the rest MMS spacecraft (Figure 2f), resulting in a smaller  $\mathbf{E} \times \mathbf{B}$  speed, we therefore infer the fast electron jet slows down at MMS 4, despite lacking of direct electron measurement. Combining with the pileup of the magnetic  $B_N$ , MMS cross the outer part of the EDR (Figure 2a).



**Figure 1.** Overview of magnetotail current sheet crossing of Magnetospheric Multiscale (MMS) 1. Panels show (a) magnetic field (geocentric solar ecliptic (GSE)), (b) ion number density, (c) ion bulk velocity (GSE) and (d) ion omnidirectional differential energy flux. Zoom-in of (e) magnetic field (LMN), (f) electric field (LMN), (g) electron number density, (h) electron bulk velocity (LMN) and (i) electron omnidirectional differential energy flux.

Intense currents, calculated from the plasma moments, are found in both the outflow direction ( $J_L$ ) and the out-of-plane direction ( $J_M$ , Figures 2g and 2h). Clear bifurcation of  $J_M$  is presented in Figure 2l. The peak of  $J_L$  is not located at the  $B_L$  reversal, but shifts into the negative  $B_L$  region (Figure 2m), consistent with the current sheet deflection due to the finite guide-field (Goldman et al., 2011). We divide this current sheet into four sublayers from the magnitude. At the two sides of this current sheet (green and brown),  $J_M$  is the major component. At the  $J_M$  dip (magenta), the current along the L direction is relatively strong, while in the shaded cyan region, both  $J_M$  and  $J_L$  are large. It is noting that in the central current sheet, electrons are primarily flowing in the field-aligned direction (Figures 2i–2k), indicating that the guide field plays a vital role in regulating the electron motion.

The thickness of this current sheet is about 70 km or four electron inertial length ( $d_e$ ,  $1 d_e \sim 18$  km) based on the spatio-temporal difference method (Shi et al., 2019), which indicates the current sheet moves southward with a varying speed from several to 40 km s<sup>-1</sup> (not shown here). Considering the change of  $B_L$  is about 9 nT crossing this current sheet, it gives  $\frac{\partial B_L}{\partial N} \sim 0.13$  nT km<sup>-1</sup>. This value reasonably agrees with that from the Ampere's Law ( $\mu_0 J_M = (\nabla \times \mathbf{B})_M = \frac{\partial B_L}{\partial N} - \frac{\partial B_N}{\partial L}$ ) if assuming the  $\frac{\partial B_L}{\partial N}$  term dominates at sublayers of large  $J_M$  (Torbert et al., 2018). Meanwhile,  $\frac{\partial B_N}{\partial L}$  becomes significant at the magnetic flux pileup region (shaded magenta region), responsible for the reduction of  $J_M$ . Based on this point, the current bifurcation would be more evident in the outer EDR, and  $\frac{\partial B_N}{\partial L}$  is  $\sim 50\%$ – $70\%$  of  $\frac{\partial B_L}{\partial N}$ . This leads into a width of the magnetic pileup region along the L direction is about 26–35 km ( $\sim 1.5$ – $2 d_e$ ), consistent with the result from particle simulations (Zenitani et al., 2011).



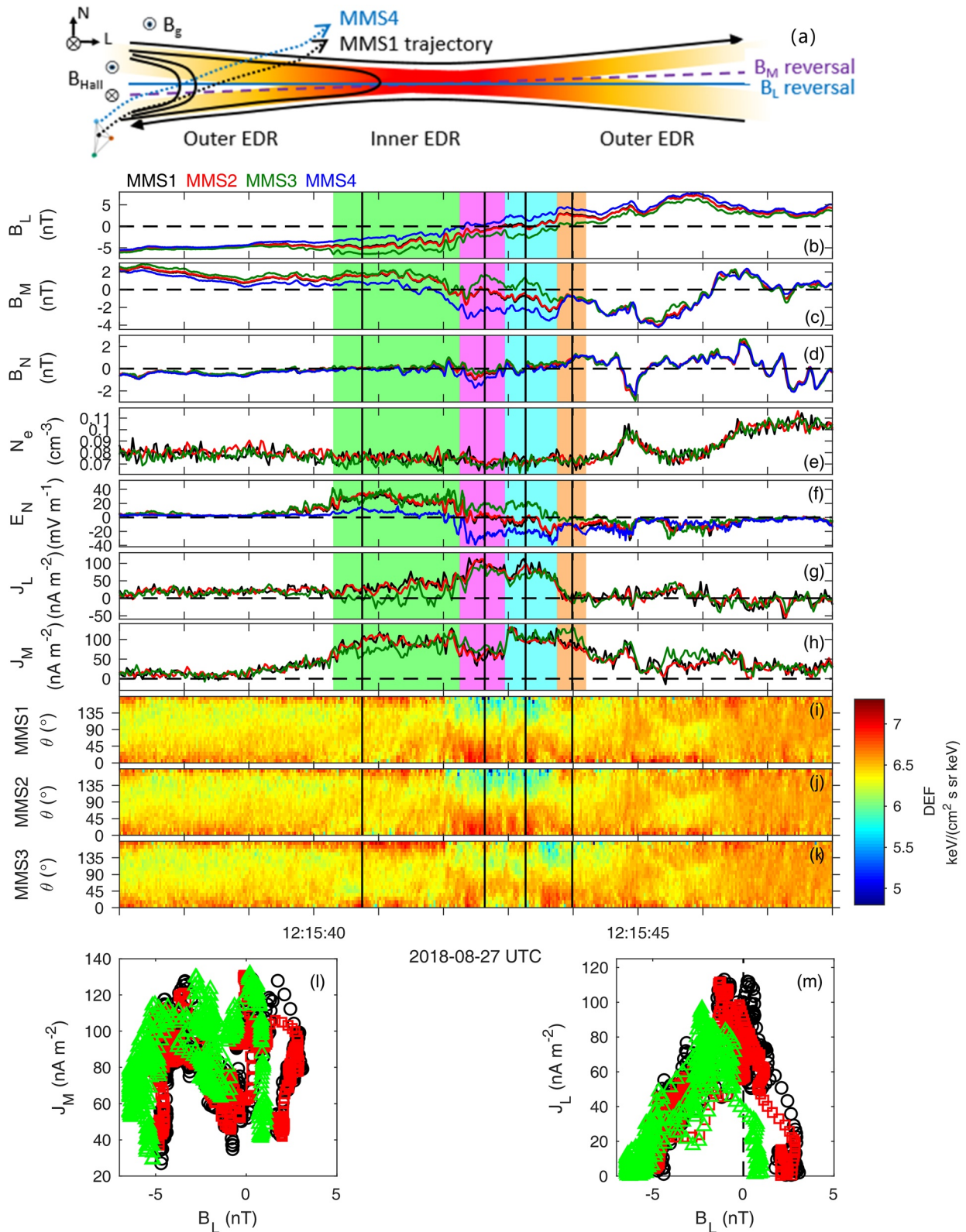


**Figure 2.** Fine structures of the electron current sheet observed by Magnetospheric Multiscale (MMS). Panels show (a) MMS relative trajectory, (b)  $B_L$ , (c)  $B_M$ , (d)  $B_N$ , (e)  $N_e$ , (f)  $E_N$ , (g)  $J_L$ , (h)  $J_M$ , (i–k) electron pitch angle spectrum from MMS 1, 2 and 3, (l–m)  $J_M$  and  $J_L$  as a function of  $B_L$ .

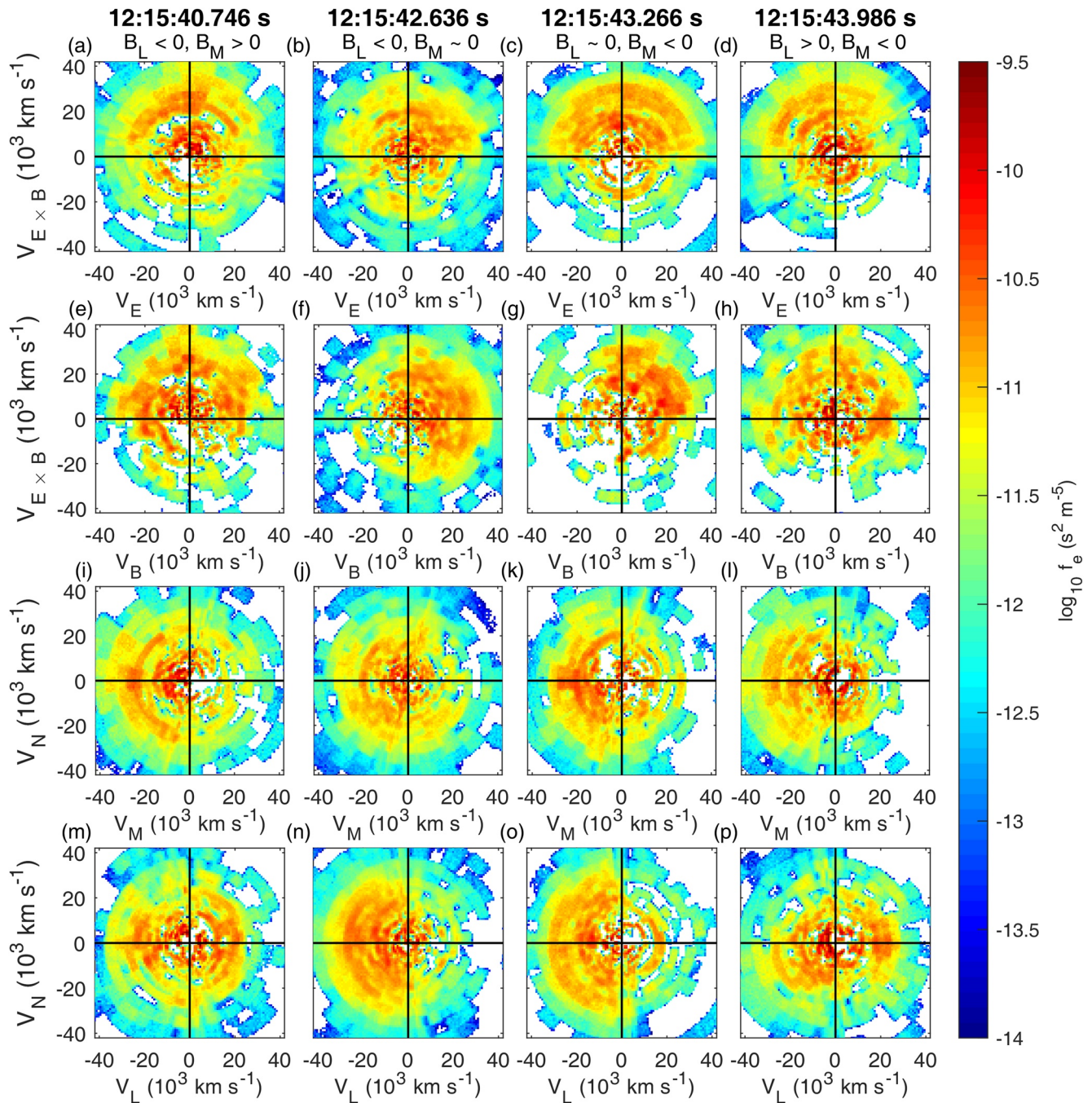


**Figure 3.** Selected electron distributions observed by Magnetospheric Multiscale 1 at the time marked by the vertical black lines in Figure 2. The top two rows are displayed in local field-aligned coordinates, and the bottom two are in fixed LMN coordinates.

Four selected electron distributions observed by MMS in different sublayers are presented in Figure 3, in which the top two rows show the reduced electron distributions in field-aligned coordinates, and the bottom two are in fixed LMN coordinates, so that we can infer sources of different current sublayers. Figure 3a shows agyrotropic crescent electron distributions perpendicular to the local magnetic field in the shaded green region, and bi-directional electrons flow along the magnetic field lines (Figure 3e). The crescent electron distributions suggest the electron meandering motion supplies the strong electron current along the M direction (Figure 3i), and the current density in the L direction is weak (Figure 3m). In the shaded magenta region, the crescent electrons have a smaller speed than that in other regions (Figure 3b), while clear parallel electron beams are observed (Figure 3f).



In this region, the magnetic field is primarily along the L direction, corresponding to a strong  $J_L$  current, and the  $J_M$  magnitude decreases. In the shaded cyan region, both clear electron crescents and parallel beams are observed (Figures 3c and 3g). Noting the multiple electron crescent also appears in the  $v_L$ - $v_N$  plane, indicating the meandering electrons are responsible for the strong  $J_L$ , while the beam electrons along the negative M direction are the main carriers of the intense  $J_M$ . This can be explained by the dominance of the finite  $B_M$  at this  $B_L$  reversal region: electrons accelerated by the reconnection electric field along the M direction form electron beams, and the meandering electrons are distorted into the  $v_L$ - $v_N$  plane. Finally, the electron motion in the shaded brown region is similar to that in the green region, and also a strong  $J_M$  related to the electron meandering motion is recorded (Figure 3d).

We have presented typical electron distributions in different sublayers, providing clues of electron orbits across the current sheet, which are different from that with zero guide-field reconnection. For reconnection with zero guide field, the electron meandering/bouncing motion at the field reversals of the current sheet dominates (i.e., Speiser, 1965), and the multiple bouncing of the accelerated electrons can form multiple electron crescents (Bessho et al., 2018; Torbert et al., 2018). In this event, similar electron meandering motion are found at the two sides of the current sheet (green and brown in Figure 3), where magnetic  $B_L$  is the major component. However, parallel electron beams appear in the central current sheet, rotating quickly from the -M direction (cyan in Figure 3k) to the -L direction (magenta in Figure 3n) with the magnetic field. This results suggest electron dynamics are effectively affected even by the relatively weak guide field ( $\sim 0.1$ ), and agree well with previous studies (i.e., Zhou et al., 2019), which show the guide field of  $\sim 0.1$  is no longer negligible in reconnection (Swisdak et al., 2005). Meanwhile, agyrotropic electron crescents that are distorted into the  $v_L$ - $v_N$  plane, are found at the  $B_L$  reversal region. The formation of the electron crescents, which is attributed to the finite  $B_M$  component, also indicates the asymmetric electron meandering/bouncing motion from side to side due to the overlapping of the guide field and Hall field. Examples of the distorted electron meandering orbits are provided by the test particle method, as seen in the supporting material. Finally, the electron crossing orbit in this current sheet can be even more complex with the absence of high-speed ( $>20,000 \text{ km s}^{-1}$ ) crescent electrons in the  $J_M$  dip region (Figure 3b), and this can be related to the energy gain/loss from the Hall electric field.

An X-line encounter of the reconnection EDR with a similar guide-field magnitude has been reported (Li et al., 2021). The reported electron current sheet can be well fitted as a Harris-type current, and the electron crescent distributions are unstable to drive large amplitude upper hybrid waves at the two sides of the current sheet. These features are different from the outer EDR crossing event here. As a comparison, complicated current structures are revealed in this event, but MMS do not observe clear activities of upper hybrid waves. This indicates that difference of electrons dynamics from the X-line region to the outer EDR, and thus a survey of the electron dynamics in reconnection EDR (zero/nonzero guide field and inner/outer part) should be performed.

### 2.3. Fluctuation of the Electron Current Sheet

Fluctuations of this current sheet, peaking at  $f \sim 5.8 \text{ Hz}$ , are observed by MMS. A highpass filter for frequencies larger than 3 Hz is applied to show the perturbed magnetic/electric field and the current density (Figure 4). The magnitude of  $\Delta B_L$  reaches to 1 nT or larger, corresponding to a spatial perturbation scale of 8 km ( $\sim 0.44 d_e$ ). Such current fluctuations can produce anomalous effect to balance the reconnection electric field. Figure 4k shows the anomalous viscosity term ( $\langle \Delta \mathbf{J} \times \Delta \mathbf{B} \rangle / \langle n_e e \rangle$ ) reaches to 0.05–0.1  $\text{mV m}^{-1}$ , contributing  $\sim 3\%$  of the reconnection electric field ( $E_R \sim 0.1 \text{ V}_{A, \text{in}} B_{L, \infty} \sim 2.5 \text{ mV m}^{-1}$ ), while the effect of the anomalous resistivity term ( $\langle \Delta n_e \Delta \mathbf{E} \rangle / \langle n_e \rangle$ ) is negligible as the electron density variation is not clear.

Combining fluctuations of current and magnetic field data, we can estimate the wave vector ( $\mathbf{k}$ ) as a function of frequency (Bellan, 2016). In order to maximize spectral resolution, we use the four-spacecraft average of  $\Delta \mathbf{B}$  and the average  $\Delta \mathbf{J}$  determined from magnetic field data using the four-spacecraft curlometer method, which leads into a phase speed ( $v_{\text{ph}}$ )  $\sim 2070 * [-0.45, -0.81, -0.37] \text{ km s}^{-1}$  in LMN (Figure 4o). This result indicates that these perturbations primarily propagate along the -M direction, or toward the tail center considering MMS locations. It is different with the flapping motion of magnetotail current sheets, which is predominantly from the center to the flanks (i.e., Erkaev et al., 2007; Sergeev et al., 2006), suggesting the source of the electron current sheet fluctuations is local.

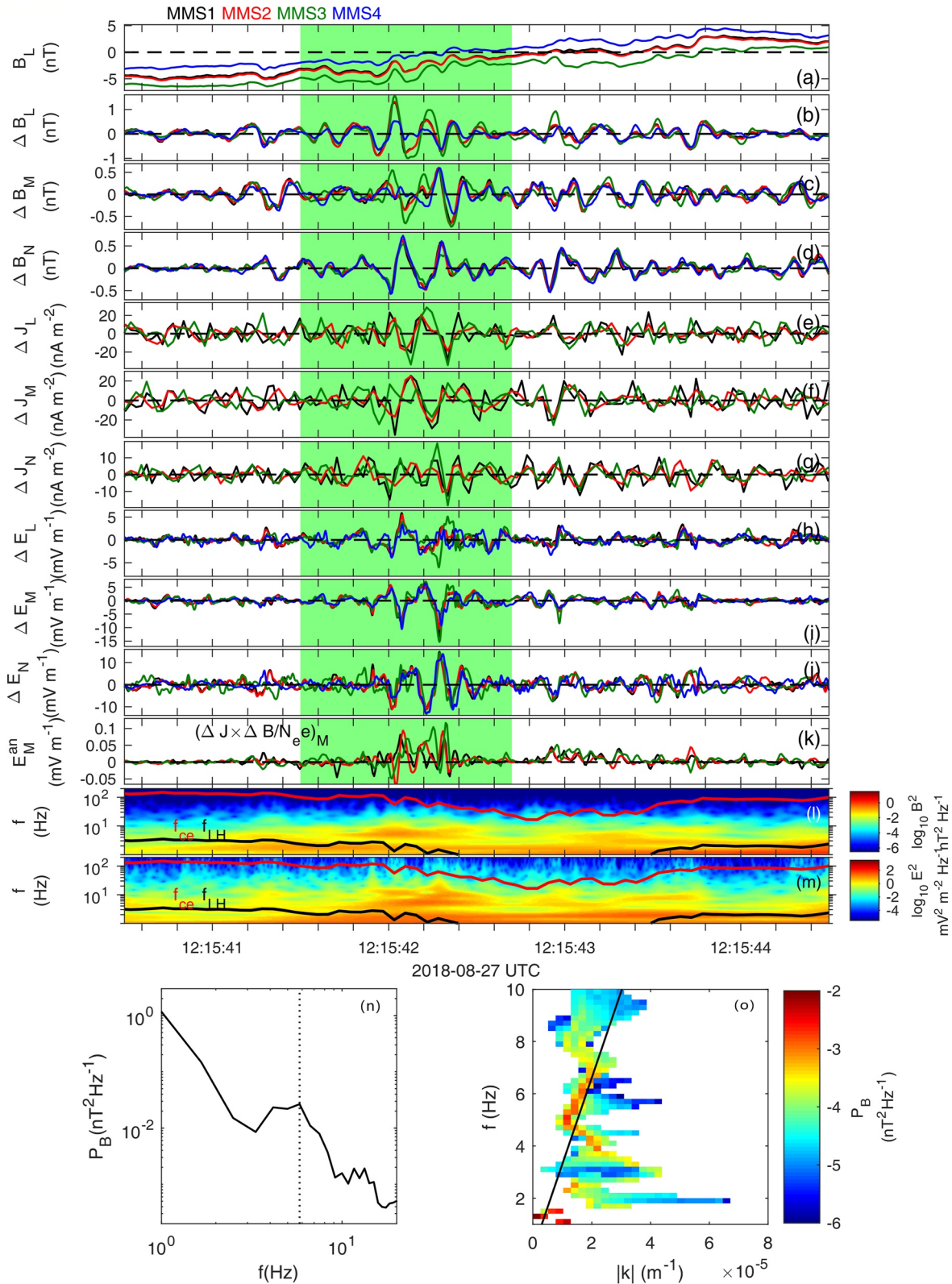


**Figure 4.** Magnetospheric Multiscale (MMS) observations of the current sheet fluctuations. (a) Magnetic  $B_L$ . Perturbations of (b–d) magnetic field, (e–g) current density, and (h–j) electric field filtered by a frequency larger than 3 Hz. (k) Anomalous electric field. (l–m) Power spectral density of the magnetic and electric field. The red and black lines indicate the electron cyclotron frequency and the lower hybrid frequency. (n) The power spectral density of the magnetic field obtained from the shaded green region, and the dotted line shows the local peak at 5.8 Hz. (o) The frequency-wave number power spectrum. The black line shows the linear fitting of the dispersion relation.

Several mechanisms for the fluctuations of electron current sheets are proposed, such as the lower hybrid drift instability (Cozzani et al., 2021; Ng et al., 2020; Wang, Chen, et al., 2021), the electron Kelvin-Helmholtz instability (Zhong et al., 2018) and the current sheet shear instability (Fujimoto & Sydora, 2017). In this outer EDR event, noticing the magnetic gradients are large in both L and N direction, we can apply the magnetic double-gradient instability, which is previously described by the single ion fluid, and has been used to explain the flapping motion of the magnetotail current sheet (Erkaev et al., 2007, 2009). Here, we apply this instability from the ion fluid to the electron fluid, as electron dynamics dominate in this thin current sheet. Though the predicted typical frequency ( $f = \frac{1}{2\pi} \sqrt{\frac{1}{\mu_0 \rho} \frac{\partial B_L}{\partial N} \frac{\partial B_N}{\partial L}} \sim 1\text{--}1.5$  Hz) from the magnetic double-gradient instability is smaller than observations, the fact that the largest perturbations are around the magnetic  $B_N$  pileup region, and these fluctuations primarily propagate along the out-of-plane ( $-M$ ) direction qualitatively agree with the observations. Therefore, the magnetic double-gradient instability is a possible candidate for the low-frequency current sheet fluctuations, and such fluctuations could be characteristic in the outer EDR, where the  $\frac{\partial B_N}{\partial L}$  is not negligible due to magnetic flux piling-up.

### 3. Summary

In this study, we have investigated an electron current sheet in the outer EDR of magnetotail guide-field reconnection. This current sheet, with a thickness of  $\sim 4 d_e$  and a maximum current intensity larger than  $100 \text{ nA m}^{-1}$ , presents some interesting features listed as follows:

1. The out-of-plane current shows clear bifurcation structures, and the entire current sheet is deflected southward due to the guide field
2. Four sublayers are found in this current sheet based on variations of the  $J_M$  and  $J_L$ . Meandering electrons and streaming electrons, which are the primary carriers of the currents, behave differently in different sublayers. Meandering electrons supply the out-of-plane current at the two sides of the current as expected, but at the  $B_L$  reversal region, the electron meandering motion are distorted into the  $v_L$ - $v_N$  plane due to the finite  $B_M$  component, indicating the guide-field ( $\sim 0.1$ ) plays an important role in modifying the electron motion
3. Low frequency fluctuations of this current sheet, propagating primarily along the out-of-plane direction with a speed of  $\sim 2000 \text{ km s}^{-1}$ , is revealed. These perturbations contribute only 3% of the reconnection electric field by the anomalous effect, suggesting the turbulence effect is weak in this event. The magnetic double-gradient instability is a candidate mechanism to drive these fluctuations, and thus such current sheet fluctuations are characteristic in the outer EDR

### Data Availability Statement

The MMS data used in this work are available at the MMS Science Data Center (<https://lasp.colorado.edu/mms/sdc/public/about/browse-wrapper/>).

### References

- Bellan, P. (2016). Revised single-spacecraft method for determining wave vector  $k$  and resolving space-time ambiguity. *Journal of Geophysical Research: Space Physics*, 121(9), 8589–8599. <https://doi.org/10.1002/2016ja022827>
- Bessho, N., Chen, L.-J., Wang, S., & Hesse, M. (2018). Effect of the reconnection electric field on electron distribution functions in the diffusion region of magnetotail reconnection. *Geophysical Research Letters*, 45(22), 12–142. <https://doi.org/10.1029/2018gl081216>
- Burch, J., Torbert, R., Phan, T., Chen, L.-J., Moore, T., & Ergun, R. (2016). Electron-scale measurements of magnetic reconnection in space. *Science*, 352(6290), aaf2939.
- Cai, H.-J., & Lee, L. (1997). The generalized Ohm's law in collisionless magnetic reconnection. *Physics of Plasmas*, 4(3), 509–520. <https://doi.org/10.1063/1.872178>
- Chen, L.-J., Daughton, W. S., Lefebvre, B., & Torbert, R. B. (2011). The inversion layer of electric fields and electron phase-space-hole structure during two-dimensional collisionless magnetic reconnection. *Physics of Plasmas*, 18(1), 012904. <https://doi.org/10.1063/1.3529365>
- Chen, L.-J., Wang, S., Hesse, M., Ergun, R., Moore, T., Giles, B., et al. (2019). Electron diffusion regions in magnetotail reconnection under varying guide fields. *Geophysical Research Letters*, 46(12), 6230–6238. <https://doi.org/10.1029/2019gl082393>
- Chen, Z., Fu, H., Wang, Z., Guo, Z., Xu, Y., & Liu, C. (2021). First observation of magnetic flux rope inside electron diffusion region. *Geophysical Research Letters*, 48(7), e2020GL089722. <https://doi.org/10.1029/2020gl089722>
- Cozzani, G., Khotyaintsev, Y. V., Graham, D., Egedal, J., André, M., Vaivads, A., et al. (2021). Structure of a perturbed magnetic reconnection electron diffusion region in the Earth's magnetotail. *Physical Review Letters*, 127(21), 215101. <https://doi.org/10.1103/physrevlett.127.215101>
- Cozzani, G., Retinò, A., Califano, F., Alexandrova, A., Le Contel, O., Khotyaintsev, Y., et al. (2019). In situ spacecraft observations of a structured electron diffusion region during magnetopause reconnection. *Physical Review E*, 99(4), 043204. <https://doi.org/10.1103/physreve.99.043204>

### Acknowledgments

This work was supported by the National Natural Science Foundation of China (grants 41731070, 41974196 and 41974170), the Chinese Academy of Sciences (QYZDJ-SSW-JSC028, XDA15052500, XDA17010301 and XDB 41000000) and the Specialized Research Fund for State Key Laboratories of China. B.-B. T. was supported by the Youth Innovation Promotion Association of the Chinese Academy of Sciences. W. Y. L. was also supported by the Youth Innovation Promotion Association, and the Young Elite Scientists Sponsorship Program by CAST and the Open Research Program of Key Laboratory of Geospace Environment CAS.



- Egedal, J., Ng, J., Le, A., Daughton, W., Wetherton, B., Dorelli, J., et al. (2019). Pressure tensor elements breaking the frozen-in law during reconnection in Earth's magnetotail. *Physical review letters*, *123*(22), 225101. <https://doi.org/10.1103/physrevlett.123.225101>
- Ergun, R., Tucker, S., Westfall, J., Goodrich, K., Malaspina, D., Summers, D., et al. (2016). The axial double probe and fields signal processing for the MMS mission. *Space Science Reviews*, *199*(1–4), 167–188. [https://doi.org/10.1007/978-94-024-0861-4\\_7](https://doi.org/10.1007/978-94-024-0861-4_7)
- Erkaev, N., Semenov, V., & Biernat, H. (2007). Magnetic double-gradient instability and flapping waves in a current sheet. *Physical review letters*, *99*(23), 235003. <https://doi.org/10.1103/physrevlett.99.235003>
- Erkaev, N., Semenov, V., Kubyshekin, I., Kubyshekina, M., & Biernat, H. (2009). MHD aspect of current sheet oscillations related to magnetic field gradients. *Annales geophysicae*, *27*(1), 417–425. <https://doi.org/10.5194/angeo-27-417-2009>
- Fujimoto, K., & Sydora, R. D. (2017). Linear theory of the current sheet shear instability. *Journal of Geophysical Research: Space Physics*, *122*(5), 5418–5430. <https://doi.org/10.1002/2017ja024079>
- Fuselier, S., Vines, S., Burch, J., Petrinc, S., Trattner, K., Cassak, P., et al. (2017). Large-scale characteristics of reconnection diffusion regions and associated magnetopause crossings observed by MMS. *Journal of Geophysical Research: Space Physics*, *122*(5), 5466–5486. <https://doi.org/10.1002/2017ja024024>
- Goldman, M., Lapenta, G., Newman, D., Markidis, S., & Che, H. (2011). Jet deflection by very weak guide fields during magnetic reconnection. *Physical review letters*, *107*(13), 135001. <https://doi.org/10.1103/physrevlett.107.135001>
- Huang, C., Du, A., & Yasong, S. G. (2020). Evolution of electron current layer during anti-parallel magnetic reconnection. *Plasma Physics and Controlled Fusion*, *62*(5), 055014. <https://doi.org/10.1088/1361-6587/ab7d49>
- Khotyaintsev, Y. V., Graham, D., Norgren, C., Eriksson, E., Li, W., Johlander, A., et al. (2016). Electron jet of asymmetric reconnection. *Geophysical Research Letters*, *43*(11), 5571–5580. <https://doi.org/10.1002/2016gl069064>
- Kuznetsova, M. M., Hesse, M., & Winske, D. (2001). Collisionless reconnection supported by nongyrotropic pressure effects in hybrid and particle simulations. *Journal of Geophysical Research*, *106*(A3), 3799–3810. <https://doi.org/10.1029/1999ja001003>
- Le, A., Egedal, J., Ohia, O., Daughton, W., Karimabadi, H., & Lukin, V. (2013). Regimes of the electron diffusion region in magnetic reconnection. *Physical review letters*, *110*(13), 135004. <https://doi.org/10.1103/physrevlett.110.135004>
- Li, W., Graham, D., Khotyaintsev, Y. V., Vaivads, A., André, M., Min, K., et al. (2020). Electron Bernstein waves driven by electron crescents near the electron diffusion region. *Nature Communications*, *11*(1), 1–10. <https://doi.org/10.1038/s41467-019-13920-w>
- Li, W.-Y., Khotyaintsev, Y. V., Tang, B.-B., Graham, D., Norgren, C., Vaivads, A., et al. (2021). Upper-hybrid waves driven by meandering electrons around magnetic reconnection x line. *Geophysical Research Letters*, *48*(16), e2021GL093164. <https://doi.org/10.1029/2021gl093164>
- Lindqvist, P.-A., Olsson, G., Torbert, R., King, B., Granoff, M., Rau, D., et al. (2016). The spin-plane double probe electric field instrument for MMS. *Space Science Reviews*, *199*(1–4), 137–165. [https://doi.org/10.1007/978-94-024-0861-4\\_6](https://doi.org/10.1007/978-94-024-0861-4_6)
- Ng, J., Chen, L.-J., Le, A., Stanier, A., Wang, S., & Bessho, N. (2020). Lower-hybrid-drift vortices in the electron-scale magnetic reconnection layer. *Geophysical Research Letters*, *47*(22), e2020GL090726. <https://doi.org/10.1029/2020gl090726>
- Phan, T., Drake, J., Shay, M., Mozer, F., & Eastwood, J. (2007). Evidence for an elongated (>60 ion skin depths) electron diffusion region during fast magnetic reconnection. *Physical review letters*, *99*(25), 255002. <https://doi.org/10.1103/physrevlett.99.255002>
- Pollock, C., Moore, T., Jacques, A., Burch, J., Gliese, U., & Saito, Y. (2016). Fast plasma investigation for magnetospheric multiscale. *Space Science Reviews*, *199*(1–4), 331–406.
- Russell, C., Anderson, B., Baumjohann, W., Bromund, K., Dearborn, D., Fischer, D., et al. (2016). The magnetospheric multiscale magnetometers. *Space Science Reviews*, *199*(1–4), 189–256. [https://doi.org/10.1007/978-94-024-0861-4\\_8](https://doi.org/10.1007/978-94-024-0861-4_8)
- Sergeev, V., Sormakov, D., Apatenkov, S., Baumjohann, W., Nakamura, R., Runov, A., et al. (2006). Survey of large-amplitude flapping motions in the midtail current sheet. *Annales geophysicae*, *24*(7), 2015–2024. <https://doi.org/10.5194/angeo-24-2015-2006>
- Shi, Q., Tian, A., Bai, S., Hasegawa, H., Degeling, A., Pu, Z., et al. (2019). Dimensionality, coordinate system and reference frame for analysis of in-situ space plasma and field data. *Space Science Reviews*, *215*(4), 1–54. <https://doi.org/10.1007/s11214-019-0601-2>
- Speiser, T. (1965). Particle trajectories in model current sheets: I. Analytical solutions. *Journal of Geophysical Research*, *70*(17), 4219–4226. <https://doi.org/10.1029/jz070i017p04219>
- Swisdak, M., Drake, J., Shay, M., & McIlhargey, J. (2005). Transition from antiparallel to component magnetic reconnection. *Journal of Geophysical Research*, *110*(A5), A05210. <https://doi.org/10.1029/2004ja010748>
- Torbert, R., Burch, J., Phan, T., Hesse, M., Argall, M., Shuster, J., et al. (2018). Electron-scale dynamics of the diffusion region during symmetric magnetic reconnection in space. *Science*, *362*(6421), 1391–1395. <https://doi.org/10.1126/science.aat2998>
- Wang, S., Chen, L.-J., Ng, J., Bessho, N., & Hesse, M. (2021). Lower-hybrid drift waves and their interaction with plasmas in a 3D symmetric reconnection simulation with zero guide field. *Physics of Plasmas*, *28*(7), 072102
- Wang, S., Wang, R., Lu, Q., Russell, C., Ergun, R., & Wang, S. (2021). Large-scale parallel electric field co-located in an extended electron diffusion region during the magnetosheath magnetic reconnection. *Geophysical Research Letters*, *48*(23), e2021GL094879. <https://doi.org/10.1029/2021gl094879>
- Webster, J., Burch, J., Reiff, P., Daou, A., Genestreti, K., Graham, D. B., et al. (2018). Magnetospheric multiscale dayside reconnection electron diffusion region events. *Journal of Geophysical Research: Space Physics*, *123*(6), 4858–4878. <https://doi.org/10.1029/2018ja025245>
- Zenitani, S., Hesse, M., Klimas, A., Black, C., & Kuznetsova, M. (2011). The inner structure of collisionless magnetic reconnection: The electron-frame dissipation measure and hall fields. *Physics of Plasmas*, *18*(12), 122108. <https://doi.org/10.1063/1.3662430>
- Zhong, Z., Tang, R., Zhou, M., Deng, X., Pang, Y., Paterson, W., et al. (2018). Evidence for secondary flux rope generated by the electron Kelvin-Helmholtz instability in a magnetic reconnection diffusion region. *Physical Review Letters*, *120*(7), 075101. <https://doi.org/10.1103/physrevlett.120.075101>
- Zhou, M., Deng, X., Tang, R., Pang, Y., Xu, X., Yuan, Z., & Huang, S. (2014). Evidence of deflected super-Alfvénic electron jet in a reconnection region with weak guide field. *Journal of Geophysical Research: Space Physics*, *119*(3), 1541–1548. <https://doi.org/10.1002/2013ja019556>
- Zhou, M., Deng, X., Zhong, Z., Pang, Y., Tang, R., El-Alaoui, M., et al. (2019). Observations of an electron diffusion region in symmetric reconnection with weak guide field. *The Astrophysical Journal*, *870*(1), 34. <https://doi.org/10.3847/1538-4357/aaf16f>